The role of order during Ogston sieving of DNA in colloidal crystals: Supplemental Information

Scott B. King and Kevin D. Dorfman*

Department of Chemical Engineering and Materials Science, University of Minnesota — Twin Cities, 421 Washington Ave. SE, Minneapolis, MN 55455

E-mail: dorfman@umn.edu

Contents

*To whom correspondence should be addressed

List of Figures

List of Tables

1 Device Fabrication and Operation

Our microfluidic devices start from soda-lime glass coated in chrome and AZ 1518 photoresist (Nanofilm). We then use a photolitographic mask with the pattern indicated in Figure 2 to pattern the photoresist as an etch mask for the Cr, which is then used as an etch mask for a buffered oxide etch [10:1 deionized (DI) water:HF] of the glass. These channels are etched to a depth of 20 μm and then diced into individual chips. Before use, the chips are cleaned in heated pirhana (1:1 H_2SO_4:H_2O_2 at 100 °C). After an hour in the bath, we rinse the chips in DI water and store the cleaned chips in DI water to preserve the hydrophilicity of the treated glass. To create the lids for the device, we form a polydimethylsiloxane (PDMS, Ellsworth Adhesives) slab on a silicon wafer that has been previously silanized with tridecafluoro-1,1,2,2,-tetrahydrooctylsilane (United Chemical Transport) to prevent adhesion of PDMS to the silicon.

Immediately prior to growing a crystal, the glass device is removed from the DI water and blown dry with filtered air. The PDMS is cut to fit the diced glass and we punch holes that match the patterned reservoirs in the glass, providing access to the channels. The PDMS is blown clean with filtered air, then rinsed by a succession of ethanol and DI water before being dried again with filtered air. Placing the PDMS in contact with the surface of the pirhana-cleaned glass makes a spontaneous, reversible bond while still allowing the channel to be wet by capillary action. Immediately after bonding, we add approximately 30 μL of DI water immediately to reservoir A (see Figure 2), which then wets the rest of the channel. We find that any delay longer than a few minutes inhibits this spontaneous wetting. After wetting, we add 30 μL of DI water to reservoirs B and C but leave reservoir D dry and open to the air.

To grow the crystal, we use the standard convective self-assembly approach.[1] We add 30 μL of a $\approx$1% w/w solution of 900 nm diameter silica colloids (Bangs Labs) to reservoirs B and C. To prevent back flow of the colloids, we also add 30 μL of DI water to reservoir A. The combination of evaporation out of reservoir D and the pressure head in the other reservoirs drives a flow towards the dry reservoir D. Changing the volume of fluid added to the reservoirs changes the flow rate towards reservoir D, while changing the relative amount of fluid added to reservoir

A changes the concentration of the colloid suspension inside the channel. This principle is shown schematically in Figure 2a. Both the flow rate and colloid concentration affect the growth rate of the crystal. (The evaporation rate out of reservoir D also affects the growth rate, but modifying this parameter requires control over both the humidity and temperature.) A quickly grown colloidal crystal generally consists of very small grains, whereas slower growth conditions promote larger grains.[2] The crystal begins to grow at the air/water interface (Figure 2c) and continues to grow backwards towards the shifted-T injection (Figure 2b). To terminate the crystal near the shifted-T injection of the device, we replace the colloid solution from reservoirs B & C with DI water.[1]

While creating the crystal, we control the crystal growth rate to produce a heterogeneous packing. It is easiest to begin with a slow growth rate, producing long-range order proceeding inward from reservoir D, and then increase the growth rate later in the crystal growth, leading to short-range order in the region near the injection point. We speed up growth by replacing the 1% colloid solution in reservoirs B and C with a 10% solution. Naturally, this approach will produce at least one interface between a region of long-range and short-range order. Since the electrophoresis measurements will take place across regions of both levels of order, we thus obtain mobility and band broadening data in both types of order with a single experiment.

2 DNA Preparation

The DNA used for these experiments are PCR amplicons of segments 709 and 86 basepairs (bp) in length obtained from the pNEB193 plasmid (New England Biolabs) using the primers [5'-TATCCGCTCACAATTCCACA-3' and 5'-AGTCGTGTCTTACCGGGTTG-3'] (709 bp) and [5'-GTCTTGAGTCCAACCCGGTA-3' and 5'-GCCTACATACCTCGCTCTGC-3'] (86 bp) (Integrated DNA Technologies) and Taq 2X Master Mix polymerase (New England Biolabs). Successful PCR amplification is confirmed by agarose gel electrophoresis. Following PCR, these amplicons are concentrated and purified by ethanol precipitation. The DNA are dyed with the intercalating fluorescent dye YOYO-1 (Invitrogen) at a dye-to-basepair ratio of 1:5 by rocking

overnight. The DNA are kept in 2.5x TBE buffer (Tris base, boric acid, and EDTA) and stored unmixed at concentrations between 10-70 μg/mL. This concentration is estimated by filtering two of the 25 PCR tubes of each batch through the Qiagen MinElute PCR purification kit and assuming the efficiency of the elution column and ethanol precipitation are similar. The concentration of the filtered DNA is calculated by measuring the absorbance of 260 nm light using a Nanodrop 2000c Spectrophotometer (Thermo Fisher Scientific). A similar measurement of the precipitated DNA gives erroneously high results, as the unbound nucleotides of the PCR mixture are not removed yet absorb at the measurement wavelength, registering a very high concentration (thousands of mg/mL). We choose the precipitation method because it allows us to reach higher stock concentrations than the Qiagen kits.

These precipitated and dyed DNA are mixed immediately prior to loading into the device, in ratios that should balance the total intensity of each injected peak. This typically requires 1 part of the 709 bp solution and 2 parts 86 bp solution. Since the stock concentration values are only estimates, the actual peak intensities are not exactly in balance (see Figure 1). For our separation measurements, the relative concentrations are more important than the absolute concentrations, as equal peaks are more easily deconvolved during full-width at half-maximum measurements.

One hour prior to performing the electrophoresis experiments, we replace the DI water in all reservoirs with 60-80 μL of 2.5x TBE supplemented with 0.07% polyvinyl pyrrolidone (Sigma Aldrich) and 0.07% ascorbic acid (Fisher-Scientific). After allowing the pressures to equilibrate for 15 minutes, platinum electrodes are inserted into each of the reservoirs and the device is pre-run for 45 minutes at $\approx$20 V/cm in the separation arm to stabilize the crystal, similar to previous work.[1] For our electrophoresis experiments, we use a LabSmith HVS448-1500 high-voltage power supply to control the potential in each of the four reservoirs. The potentials are calculated in our custom LabView controller by treating the device as four conductors of resistivity ρ, fluid cross-sectional area A available for conduction, and length L, with a shared junction and conserving current. We also take care to account for the non-uniform resistivity of the crystal in the separation arm by treating that "wire" as two resistors in series, where the resistance of each section of the

wire, $R_i = \rho L_i / A_i$, accounts for both its length and the cross-sectional area available for conduction through the fluid. After 45 minutes of pre-running, the electric fields are turned off and the DNA solution is loaded by first removing 30 μL of running buffer from reservoir B and replacing it with 30 μL of dyed DNA solution. The DNA are loaded using the standard shifted-T protocol,[3] and the typical injection width is $\approx$100 μm.

3 Confirmation of Ogston Regime

We confirm here that our experiments indeed take place in the Ogston sieving regime. While a colloidal crystal possesses at least short-range ordering, the model only requires specifying the fractional volume available to the DNA. However, it is important that the DNA be small compared to the size of the pores. Using a wormlike chain model for the DNA[4] with a persistence length of 53 nm[5] and assuming a 30% increase in contour length from the intercalating fluorescent dye,[6–8] we find $R_{g,86} = 10$ nm and $R_{g,709} = 59$ nm. Zeng and Harrison[1] proposed to use a value of 15% of the colloid diameter d to roughly represent the size of the throat connecting interstitial spaces of the crystal, based on fitting a touching sphere. The throats are narrower than the interstitial spaces, which correspond to 41.4% of the colloid diameter for a site of octahedral coordination and 22.5% for tetrahedral coordination and are periodically distributed.[9] However, the 15.5% width of the throats form a useful limiting case for our interests. With a nominal colloid diameter of 900 nm, the throat size corresponds to a radius of 70 nm. The radii of gyration of our DNA are smaller than the narrowest pore space inside the crystal, and much smaller than the centers of the pores. Thus, from a geometric perspective, our experiments are taking place in the Ogston sieving regime.

In addition to satisfying the geometric criterion, it is also essential to confirm that we satisfy the dynamic criterion of the Ogston sieving theory. The assumption that the mobility is proportional to the fractional volume available to the DNA requires that the DNA be able to sample its configurational space during the transit through a given pore. In other words, the Ogston sieving model applies to near-equilibrium separations. Similar geometries can yield non-intuitive behavior[10,11]

when the transit time is shortened due to a strong electric field and the separation is far from equilibrium. To assure the molecules have sufficient time to sample these spaces, we can compare their convection time to their self diffusion time, otherwise known as the Péclet number. The fastest molecule we measured has a speed of nearly 50 μm/s, which travels the interplanar spacing distance in $\tau_v = 1.5 \times 10^{-2}$ s. Using diffusion coefficients calculated via the wormlike chain theory of Yamakawa and Fujii[12] ($D_{86} = 34.9$ μm^2/s, $D_{709} = 7.9$ μm^2/s, assuming a viscosity of 1 cP and $T = 298$ K), we arrive at self-diffusion times of $\tau_{s,86} = 3.0 \times 10^{-6}$ s and $\tau_{s,709} = 4.5 \times 10^{-4}$ s. The corresponding Péclet numbers, $\mathrm{Pe}_{86} = 2 \times 10^{-4}$ and $\mathrm{Pe}_{709} = 3 \times 10^{-2}$, are both small compared to unity. As a result, the dynamic assumption of the Ogston sieving model is satisfied.

Finally, we also need to confirm that the regions with short-range order and those with long-range order have the same pore sizes. The laser diffraction measurements provide a very convenient way to address this question, since the laser diffraction patterns are analogous to a Fourier transform of the three-dimensional correlations of each colloid within the spot of the laser beam. A perfectly-ordered colloidal crystal diffracts into clean, bright spots. We see this in Figure 3a, implying that within the entire area of the beam, each colloid's nearest-neighbor orientations are identical. If, instead, we have within our interrogating beam many small grains with unique orientations, each grain will have their diffraction spots at unique rotation relative to the other grains. Overlaying many of these patterns will yield a diffraction ring as seen in Figure 3c, and implies that within our beam there are many changes in crystalline orientation. However, the first-order diffraction information (either spots or rings) is located at the same distance, which confirms a consistent nearest-neighbor distance. Our columns are thus close-packed, independent of the long-range ordering, implying a uniform pore size throughout the medium.

4 Supplemental Figures and Tables

Table S1: Experimental details for the chips in Figure S1. The rings correspond to mini-columns with short-range order, and the spots correspond to mini-columns with long-ranged order. The crystal start location indicates the location where the crystal starts relative to center of the shifted-T injection while the crystal finish is the total length of the elution column after placement of the PDMS reservoir hole (overlapping the channel). The measurement start location indicates the left-most position of the bars in Figure S1. In some columns, we made multiple elutions at the indicated electric fields.

Chip	Rings	Spots	Crystal Location		Measurement Window		Electric Fields (V/cm)
			Start (mm)	End (mm)	Start (mm)	End (mm)	
1	4	10	0.6	22.7	11.1	17.7	17.6
2	7	9	0.6	23.4	10.6	17.8	18.5
3	7	9	0.6	22.8	10.5	18.1	20 (x5)
4	8	8	1.1	22.0	10.1	17.8	21.2 (x2)
5	8	8	0.8	22.3	10.5	18.5	11.4, 20.1, 28.8
6	8	9	1.1	22.4	10.5	18.3	12.0 (x2), 21.1, 30.2
7	9	8	1.5	22.8	14.5	22.3	18.7 (x3), 27.6 (x2)

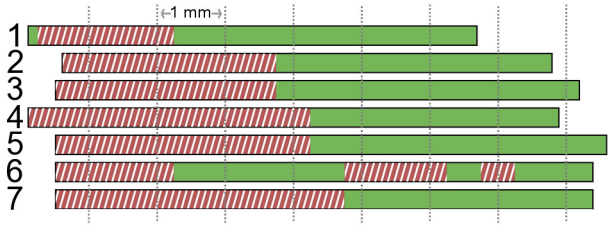

Figure S1: Schematic depiction of the regions of long-range order and short-range order in the 7 chips used for the experiments. The color code indicates the type of crystalline order in a given 0.5 mm mini-column, with red hashes and green solids signifying “rings" (short-range order) and “spots" (long-range order), respectively. Examples of each type of ordering are presented in Figure 3. The dashed lines indicate the locations of every other ruler marker in Figure 2. The leftmost line is the first 1 mm position marker; the exact distance from the injection can be found in Table S1. Each elution column is marked to the left with its chip number.

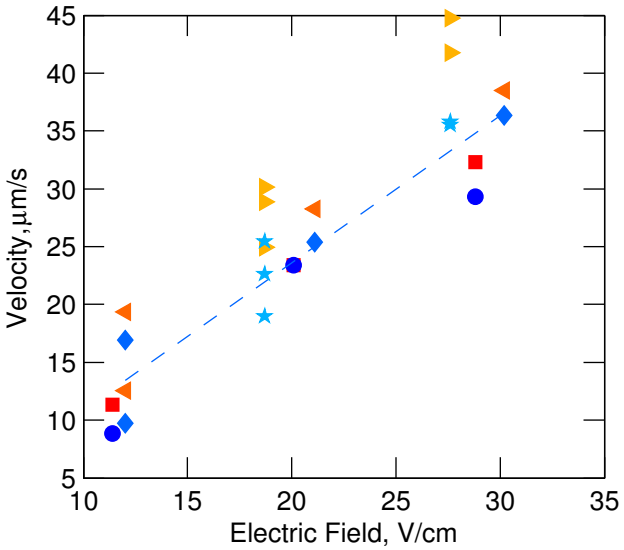

Figure S2: Plot of the velocity vs. electric field confirms a linear scaling, characteristic of Ogston sieving, for the three different chips in which multiple fields were tested (chips 5-7). The line shown is a fit of the data from Chip 6, 709 bp DNA ($\diamond, R^2 = 0.93$). The R^2 values for the other fits are: Chip 5, 86 bp ($\square, R^2 = 0.99$); Chip 5, 709 bp ($\circ, R^2 = 0.94$); Chip 6, 86 bp ($\triangleleft, R^2 = 0.94$); Chip 7, 86 bp ($\triangleright, R^2 = 0.94$); Chip 7, 709 bp ($\star, R^2 = 0.91$).

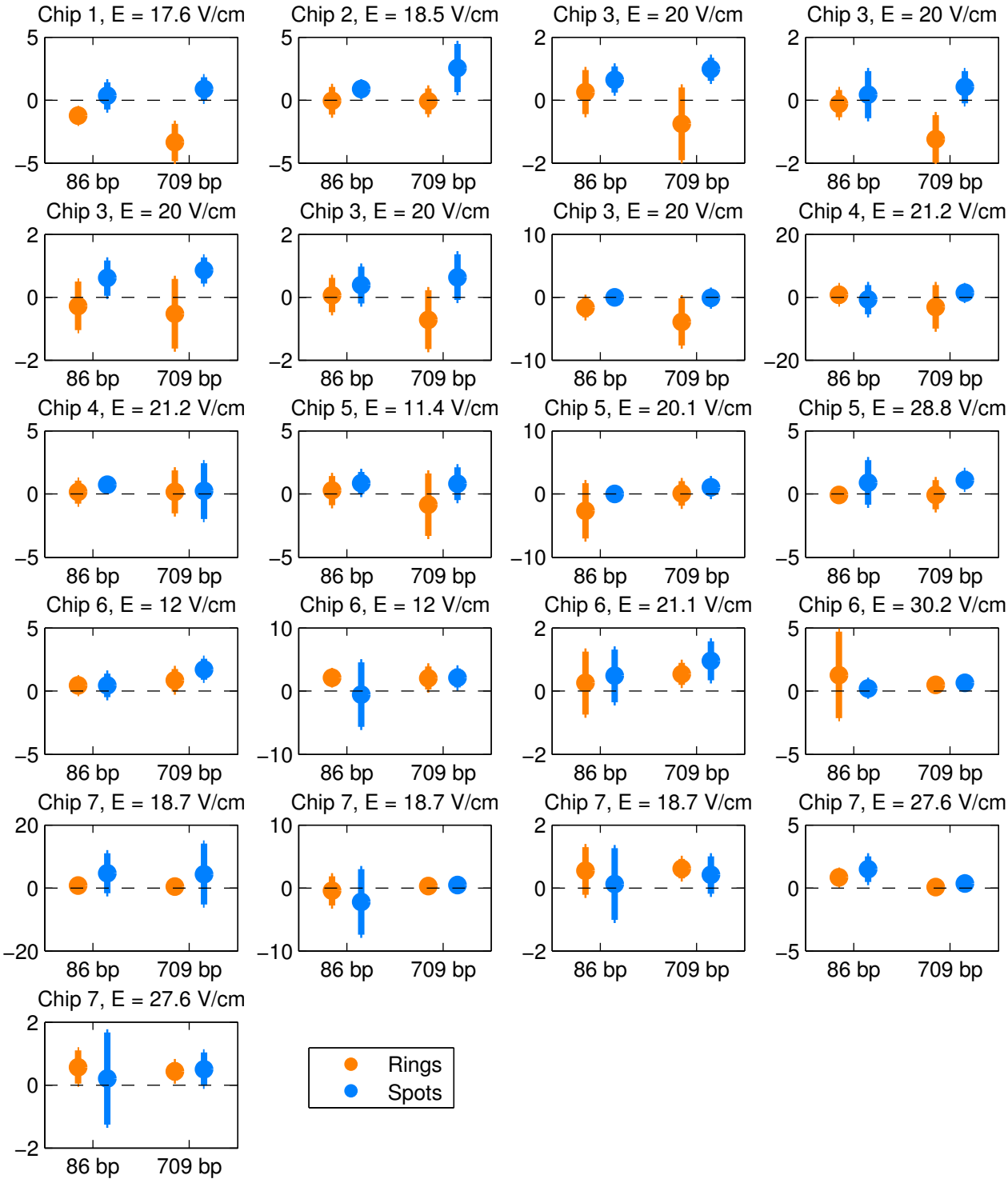

Figure S3: The average change in the FWHM across a mini-column in seconds, sorted by DNA size and crystal quality. The error bars correspond to one standard deviation of the mean.

References

(1) Zeng, Y.; Harrison, D. J. *Anal. Chem.* **2007**, *79*, 2289–2295.

(2) Kim, E.; Xia, Y.; Whitesides, G. M. *Adv. Mater.* **1996**, *8*, 245–247.

(3) Jacobson, S. C.; Hergenroder, R.; Koutny, L. B.; Warmack, R. J.; Ramsey, J. M. *Anal. Chem.* **1994**, *66*, 1107–1113.

(4) Rubinstein, M.; Colby, R. H. *Polymer Physics*; Oxford University Press: New York, 2003.

(5) Bustamante, C.; Marko, J. F.; Siggia, E. D.; Smith, S. *Science* **1994**, *265*, 1599–1600.

(6) Perkins, T. T.; Smith, D. E.; Larson, R. G.; Chu, S. *Science* **1995**, 83–87.

(7) Bakajin, O. B.; Duke, T. A. J.; Chou, C. F.; Chan, S. S.; Austin, R. H.; Cox, E. C. *Phys. Rev. Lett.* **1998**, *80*, 2737–2740.

(8) Randall, G. C.; Doyle, P. S. *Macromolecules* **2005**, *38*, 2410–2418.

(9) Barsoum, M. W. *Fundamentals of Ceramics*; Institute of Physics: London, 1997.

(10) Gauthier, M. G.; Slater, G. W. *Electrophoresis* **2003**, *24*, 441–451.

(11) Laachi, N.; Declet, C.; Matson, C. M.; Dorfman, K. D. *Phys. Rev. Lett.* **2007**, *98*, 098106.

(12) Yamakawa, H.; Fujii, M. *Macromolecules* **1973**, *6*, 407–415.